ChemPlusChem

Research Article
doi.org/10.1002/cplu.202400242

Chemistry Europe
European Chemical Societies Publishing

www.chempluschem.org

# NDT-C11 as a Viable Novel Detergent for Single Particle Cryo-EM

Chimari Jiko[+],[a] Jiannan Li[+],[b] Youngsun Moon[+],[c] Yoshito Tanaka,[d] Chai C. Gopalasingam,[e] Hideki Shigematsu,[f] Pil Seok Chae,[c] Genji Kurisu,[b] and Christoph Gerle*[e]

Single particle cryo electron microscopy (cryo-EM) is now the major method for the determination of integral membrane protein structure. For the success of a given project the type of membrane mimetic used for extraction from the native cell membrane, purification to homogeneity and finally cryo-grid vitrification is crucial. Although small molecule amphiphiles – detergents – are the most widely used membrane mimetic, specific tailoring of detergent structure for single particle cryo-EM is rare and the demand for effective detergents not satisfied. Here, we compare the popular detergent lauryl maltose-neopentyl glycol (LMNG) with the novel detergent neopentyl glycol-derived triglucoside-C11 (NDT-C11) in its behavior as free detergent and when bound to two types of multisubunit membrane protein complexes – cyanobacterial photosystem I (PSI) and mammalian F-ATP synthase. We conclude that NDT-C11 has high potential to become a very useful detergent for single particle cryo-EM of integral membrane proteins.

## Introduction

The biomembrane is a universal, essential part of cellular life and to understand its structure, and function is a key aim of the life sciences.[1] The active, energy, matter and information transducing component of cellular membranes are integral membrane proteins (IMPs) that span the amphiphilic lipid bilayer of the biomembrane, and are consequently also of amphiphilic nature.[2] The amphiphilic surface of integral membrane proteins greatly complicates; extraction from their native cell membranes, purification to homogeneity, and performance of *in vitro* experiments.[3] These experimental challenges frustrate biomedical investigations that aim to exploit the fact that more than 50% of marketed drugs are targeting integral membrane proteins.[4] This is especially true for high resolution structure determination by X-ray crystallography, due to the difficulties of accommodating the formation of robust crystal contacts with the amphiphilic surface of integral membrane proteins.[5] As a consequence, the number of IMP structures deposited in the Protein Data Bank (PDB)[6] lags far behind that of water soluble proteins (Protein Data Bank Japan: https://pdbj.org; Stephen White database of Membrane Proteins of Known 3D Structure: https://blanco.biomol.uci.edu/mpstruc).[7] Moreover, IMP structures determined by X-ray crystallography at resolutions of better than 2.0 Å still remain rare. The latter is problematic, because resolution matters. A firm structural basis for understanding IMP function requires the clear visualization of bound waters and ligands, which is difficult to obtain at resolutions worse than 2.0 Å. This is particularly pertinent for structure based drug design, where accurate poses of bound drug compounds are prerequisites to guide new rounds of compound development.

Single particle cryo-EM is a method for the determination of large macromolecules (>50 kDa) that negates the need for crystallization, whereby since the advent of the 'Resolution Revolution' the technique has been increasingly employed to determine IMP structures at so called 'crystallographic resolution'.[8,9] The widespread popularity of single particle cryo-EM coupled with significant improvements in instrumentation and image processing suites in recent years, have now made

[a] *Prof. C. Jiko[+]*
*Institute for Integrated Radiation and Nuclear Science*
*Kyoto University*
*Kumatori, Osaka 590-0494, Japan*

[b] *Dr. J. Li,[+] Prof. G. Kurisu*
*Institute for Protein Research*
*Osaka University*
*Suita, Osaka 565-0871, Japan*

[c] *Y. Moon,[+] Prof. P. S. Chae*
*Department of Bionano Engineering*
*Hanyang University*
*Ansan 155-88, South Korea*

[d] *Y. Tanaka*
*Graduate School of Life Science*
*University of Hyogo*
*Kamigori 678-1297, Japan*

[e] *Dr. C. C. Gopalasingam, Dr. C. Gerle*
*Life Science Research Infrastructure Group*
*RIKEN SPring-8 Center*
*Sayo 679-5148, Japan*
*E-mail: christoph.gerle@riken.jp*

[f] *Dr. H. Shigematsu*
*Structural Biology Division*
*Japan Synchrotron Radiation Research Institute*
*SPring-8, Sayo 679-5148, Japan*

[+] *Shared first author*

*Supporting information for this article is available on the WWW under https://doi.org/10.1002/cplu.202400242*

single particle cryo-EM not only the dominant technique for structure determination of IMPs (in terms of annual PDB entries), but has also rendered map resolutions of ~2.0 Å more feasible.[3,10,11] It is anticipated that within the near future most experimental structure determination of IMPs will be done using cryo-EM. Both structure determination by X-ray crystallography and single particle cryo-EM requires the use of membrane mimetics for the *in vitro* stabilization of IMPs outside their native environment of the biomembrane.[12] Current membrane mimetics that are in use by the community are Membrane Scaffold Protein-based nano-discs, amphipols, styrene-maleic acid lipid particles (SMALPs), saposin-lipid-protein (Salipro), bicelles and small molecule amphiphiles, i.e., detergents.[13,14]

Among these membrane mimetics, detergents are the most prevalent and popular, due to their usability in all experimental steps from extraction, over purification and up till final sample preparation for data collection.[15] With X-ray crystallography having been the dominant method for structure determination of IMPs since the report of the first atomic model of the bacterial reaction center in 1985,[16] the development and use of detergents has been largely formed by the technical requirements of growing highly ordered 3D crystals of sufficient size and quantity for the collection of X-ray diffraction data.[17] Some of the earlier examples of detergents in IMP research, like lauryldimethylamine-*N*-oxide (LDAO) and cholate, are ionic, which were followed in the 1980s by milder, less disruptive non-ionic detergents, with n-octyl-β-D-glucoside (OG) and n-dodecyl-β-D-maltopyranoside (DDM)[18] being among the most successful (Figure 1). These two popular, non-ionic detergents showcase the conflict between preserving IMP stability by exploiting the milder properties of a longer chained detergent, like DDM, and a small protein-detergent-complex (PDC) that favors crystal contact formation, enabled by a shorter chained detergent like OG. The development of novel, lipid like detergents such as lauryl maltose-neopentyl glycol (LMNG)[19] and glyco-diosgenin (GDN)[20] from the 2000s onwards opened the door to *in vitro* studies of IMPs, whose stability and integrity cannot be easily preserved in conventional, single chained non-ionic detergents such as DDM (see Table 1 for a list of basic physical properties of these detergents). The introduction of LMNG and GDN proved to be an important step for the study of biomedically relevant and often very fragile IMPs of mammalian origin such G-protein coupled receptors, transporters or energy converters (Figure 1). Though the large PDC of LMNG and GDN is a challenge for growing highly ordered 3D crystals for X-ray crystallography, both LMNG and GDN had great potential for their application to single particle cryo-EM. That potential was fully realized, after it was known that their very low critical micellar concentration (CMC) and high affinity PDC could avoid the typically detrimental effects on cryo-EM experiments which free detergent micelles cause, like diminishing image contrast and complications in thin ice formation. These free micelles could now be easily removed or reduced without causing IMP aggregation.[21] Introduced to single particle cryo-EM in 2015[21] and 2017[22] respectively, LMNG and GDN are now among the most popular membrane mimetics for IMP vitrification in single particle cryo-EM.[3] In fact, in the last two years for studies that reported a better than 3 Å resolution LMNG, GDN and DDM were the most frequently used membrane mimetics for cryo-grid vitrification.[23]

What are the properties of an ideal detergent that fulfills the various requirements for high resolution structure determination by single particle cryo-EM? As listed in Table 2, an ideal detergent does indeed need to satisfy many requirements, but it also shows that LMNG comes quite close and that room for improvement is well defined. Among the known issues in the use of LMNG are its tendency to form highly elongated free detergent micelles.[21,24,25] This is a nuisance when concentrating IMPs to levels of ~5–15 mg/ml, as often required for cryo-grid vitrification, or buffer exchanges using centrifugal concentrators. Perhaps connected to its peculiar formation of tubular micelles, some IMPs, e.g. photosystems, exhibit sub-optimal monodispersity in LMNG.[26] Furthermore, though LMNG is

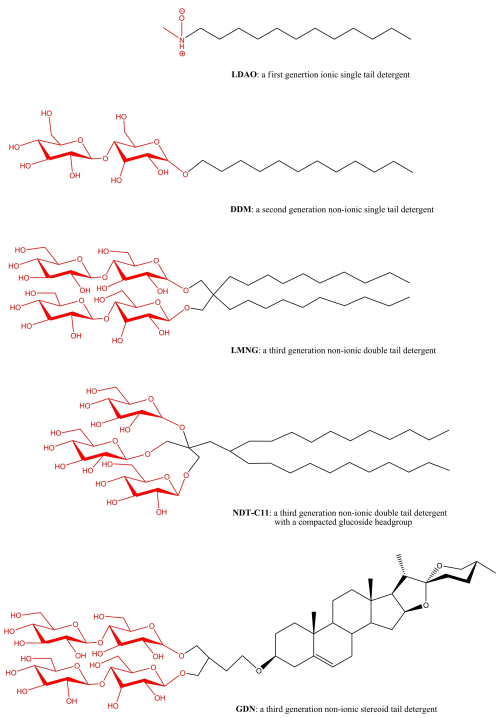


**Figure 1.** Chemical structures of the IMP research common detergents, LDAO, DDM, LMNG, GDN and the novel NDT-C11. Headgroups are depicted in red.

**Table 1.** Some basic physical properties of detergents relevant to this study.[18,19,20,30] Note that the micelle size (hydrodynamic radius; $R_h$) and shape for LMNG is concentration dependent and for higher concentrations as shown in Figure 2a, cannot be described accurately by the hydrodynamic radius alone.

| Amphiphile | MW (Da) | CMC[a] | $R_h$ (nm)[b] |
|---|---|---|---|
| DDM | 510.6 | 0.0087 % | 3.5 ± 0.04 |
| LMNG | 1,005.2 | 0.0010 % | 7.2 ± 0.01 |
| GDN | 1,165.3 | 0.0021 % | 3.86 ± 0.05 |
| NDT-C11 | 959.2 | 0.0005 % | 3.5 ± 0.0 |

[a] critical micellar concentration ($H_2O$, w/w). [b] hydrodynamic radius.

**Table 2.** A list of desired properties of an ideal detergent for the use in cryo-grid vitrification for single particle cryoEM.

| Ideal properties of a detergent in single particle cryoEM |
|---|
| conveys the same complex stability as the native membrane |
| provides monodispersity |
| promotes random orientation in a thin film of buffer |
| allows removal of free detergent micelles |
| promotes formation of stable thin buffer film over holes |
| protects against the air-water interface |
| easy to exchange against a primary detergent |
| allows quick concentration/buffer exchange by concentrators |
| keeps lipids bound |
| good solubility and stable stock solution |
| economic price |

superior to the gold standard non-ionic detergent DDM in stabilizing IMPs, it lacks the ability to preserve the highly fragile interactions of higher order oligomers, such as those in the mammalian F-ATP synthase tetramer.[27–29] Since the length of LMNG double alkyl chain has already been optimized to C12 in the original work on the MNG series,[19] promising targets in the structure of LMNG for improvement of its molecular properties in single particle cryo-EM are the hydrophilic headgroup and the tail connecting linker region.

NDT-C11 was developed as a variant of LMNG with a more compact hydrophilic triglucoside headgroup and a novel neopentyl glycol linker (Figure 1).[30] Stability tests on bacterial transporters performed in the original study indicated that NDT-C11 confers greater stability than the bench mark detergent DDM. Testing of novel detergents for their use in single particle cryo-EM is costly and time consuming. Consequently, the successful introduction of novel detergents in single particle cryo-EM of IMPs is mostly slow and often needs to be initiated by successful example studies. This is especially true, if the detergent in question is not commercially available, as it is the case for NDT-C11. Given the promising properties of NDT-C11 reported in the original report and the unsatisfied demand in the field for viable novel detergents, we set out to test the usefulness of NDT-C11 for single particle cryo-EM. In particular, we wanted to know if this variant of LMNG is overcoming at least one of the weaker aspects of this maltoside detergent for single particle cryo-EM of IMPs.

Here, we report our results on comparing NDT-C11 to LMNG in its free micellar form and when bound to cyanobacterial photosystem I (PSI) and mammalian F-ATP synthase. We conclude that NDT-C11 has high potential as an important novel detergent for single particle cryo-EM of IMPs.

## Results and Discussion

### NDT-C11 in Free Form

Transmission electron microscopy is a straightforward way for the direct visualization of the shape and size of free detergent micelles. That this approach works well for LMNG had previously been shown both by negative stain and cryo electron microscopy, demonstrating that free micelles of LMNG can be of very long, tube-like shape,[21,24] a finding that is supported by small-angle X-ray scattering (SAXS).[25]

We first asked, if NDT-C11, in analogy to LMNG, also forms elongated free micelles at high detergent concentration. To that end, we prepared 1% (w/w) solutions of NDT-C11 and LMNG in MilliQ water and imaged thin films of these solutions after standard plunge freezing in liquid ethane. For LMNG the expected tube-like free micelles of several hundred nanometer length were visualized (Figure 2a). To estimate the diameter of the tube-like micelles we performed 2D image classification on boxed regions of the tube-like micelles, which indicates a diameter of 4.0 nanometer (Figure 2a, inset). The previously reported diameter of the hydrophobic region of LMNG micelles at 1% concentration, which was obtained from SAXS measurements, is considerably shorter at 2.8 nanometer.[25] The larger value found here is likely due to the fact that in our cryo-EM micrograph based measurements both the hydrophobic core and the hydrophilic headgroup region of the free detergent micelle contributes to electron scattering. For NDT-C11 no elongated micelles could be detected and the visualized spherical micelles had an apparent size of 3.5 nanometer as estimated from 2D class averages of the detergent micelle (Figure 2b). To our surprise, the estimated diameter of 3.5 nanometer is identical to the result obtained by dynamic light scattering.[30] Since cryo-EM image classification and dynamic light scattering both arrived at the same value, despite being considerably differing methods to size estimation, we are confident that our 2D classification based estimate for LMNG and NDT-C11 micelle diameters is essentially correct. These results suggest that NDT-C11, unlike LMNG, does not pose experimental inconveniences for protein concentration or buffer exchange by the formation of tube-like free detergent micelles when using standard centrifugal concentrators.

Next, we wanted to probe if the presence of free detergent micelles becomes negligible at concentrations that are still clearly above the CMC of NDT-C11, which based on a fluorescence dye assay was reported to be 0.0005% (w/w).[30] Using negative stain electron microscopy we imaged a dilution series of NDT-C11 solubilized in a standard buffer (Figure 3). The results clearly showed that already at 0.005%, i.e., 10 times above CMC, the presence of free detergent micelles becomes insignificant. This is important for successful vitrification of NDT-C11-stabilized IMPs, since the presence of large amounts of free detergent micelles can be detrimental for obtaining good image contrast and tends to complicate cryo-grid vitrification.[21,31,32] These results demonstrate that NDT-C11 in its free form is superior to LMNG in regard to its experimental

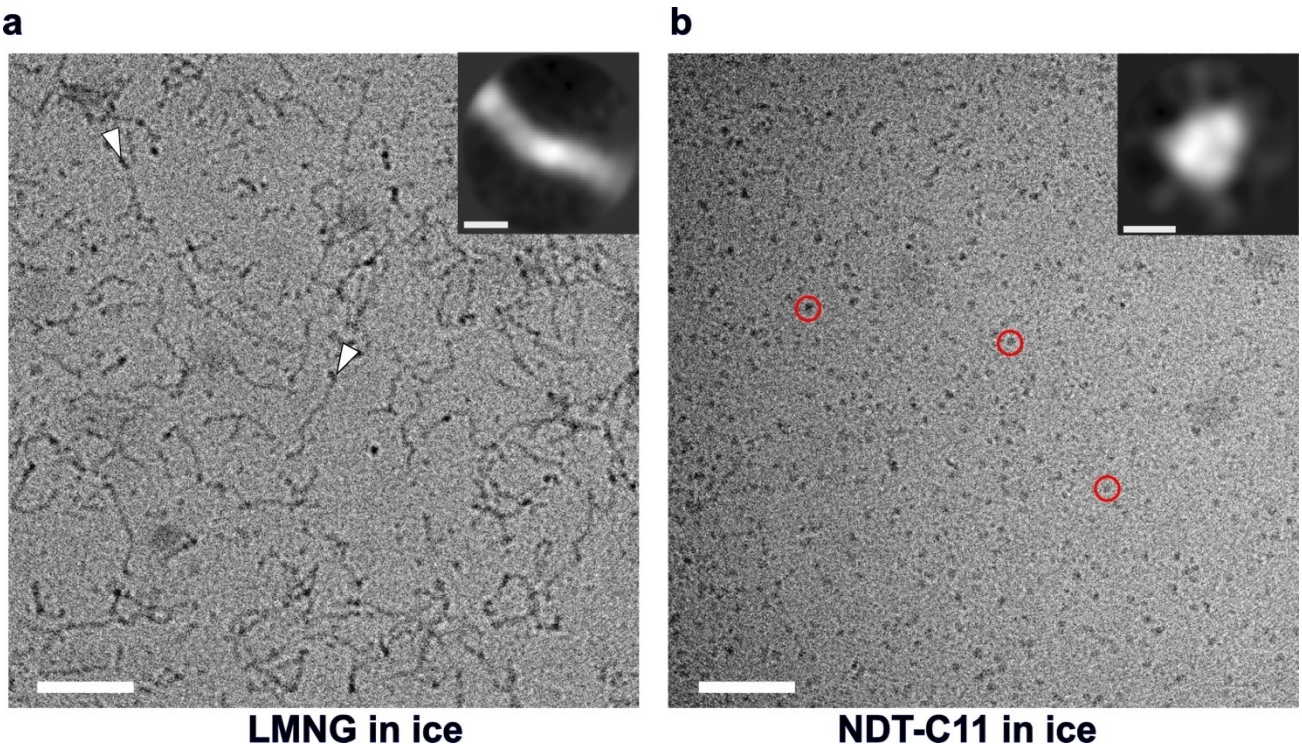


**Figure 2.** Free detergent micelles in vitreous ice. Representative cryo-images of (a) LMNG solubilized in water at a concentration of 1% (w/w) with two tube-like micelles indicated by white triangles. Inset: 2D class of tube-like micelles. (b) Vitrified NDT-C11 with three spherical micelles encircled in red. Inset: 2D class of spherical micelles. Scale bars: 50 nm for the raw micrographs in (a) and (b), 50 nm for the LMNG 2D class of the inset in (a) and 25 nm for the NDT-C11 2D class of the inset in (b).

handling, encouraging further testing of its compatibility with IMP single particle cryo-EM.

### NDT-C11 and Cyanobacterial PSI

Photosystem I (PSI) is one of the two large light energy converting multisubunit membrane complexes that perform the light reactions of photosynthesis.[33] Cyanobacterial photosystem I from *T. elongatus* was the first PSI whose structure was determined to high resolution (2.5 Å) by X-ray crystallography 25 years ago.[34] Recently, it was demonstrated that single particle cryo-EM can deliver high resolution, i.e., better than 2.0 Å, structures of cyanobacterial PSI even when bound with the electron acceptor ferredoxin.[35] A feat achieved despite the relatively modest image data set of 3,018 recorded and 1,959 analyzed movies.[35,36] Key to this improvement for high resolution structure determination of the *T. elongatus* PSI trimer was sample preparation using GDN at highly reduced concentration as the vitrification detergent. GDN was chosen over LMNG as the detergent for vitrification, because a prior study of the *T. elongatus* PSI monomer had indicated that in the presence of LMNG monomeric PSI particles tend to form elongated microaggregates, preventing good dispersion for cryo-grid imaging.[26,37] A similar finding occurred for algal PSI from *Chlamydomonas reinhardtii* (Sup. Figure 1).[38] This apparent incompatibility of LMNG with single particle cryo-EM analysis of PSI was disappointing and prompted us to ask whether the LMNG variant, NDT-C11, might lead to a different outcome.

Toward this aim, we conducted *T. elongatus* PSI purification as previously described, however, exchanged detergent in the last sucrose density gradient (SDG) to either NDT-C11 or LMNG. The SDG was also employed to reduce free detergent micelles to a negligible level by the GraDeR[21] approach, which previously, when using GDN or LMNG, worked well without any detectable precipitation occurring. Even in the presence of only 0.005% NDT-C11 in the gradient buffer, a sharp green band of PSI complexes could be observed validating the expectation that the low CMC of NDT-C11 allows for the removal of basically all free detergent micelles without causing protein complex precipitation (Figure 4a). When using DDM for the SDG the detergent concentration had to be kept well above the CMC at 0.05% to avoid PSI complex precipitation, i.e., the presence of fairly large amounts of free detergent micelles were required. After recovery of the green PSI band and removal of sucrose using centrifugal concentrators, we wanted to obtain insights into the aggregation state and level of free detergent micelles of the NDT-C11 SDG, using mass photometry.

Mass photometry is a powerful method to obtain detailed insights into protein complexes in bulk solution, however, for usable measurements the required protein concentration is far lower than the 1 to 10 mg/ml range that is typically used in single particle cryo-EM. Additionally, the presence of large amount of free detergent micelles precludes successful mass photometric measurements.[39,40] Therefore, for mass photo-

Research Article
doi.org/10.1002/cplu.202400242
Chemistry Europe
European Chemical Societies Publishing

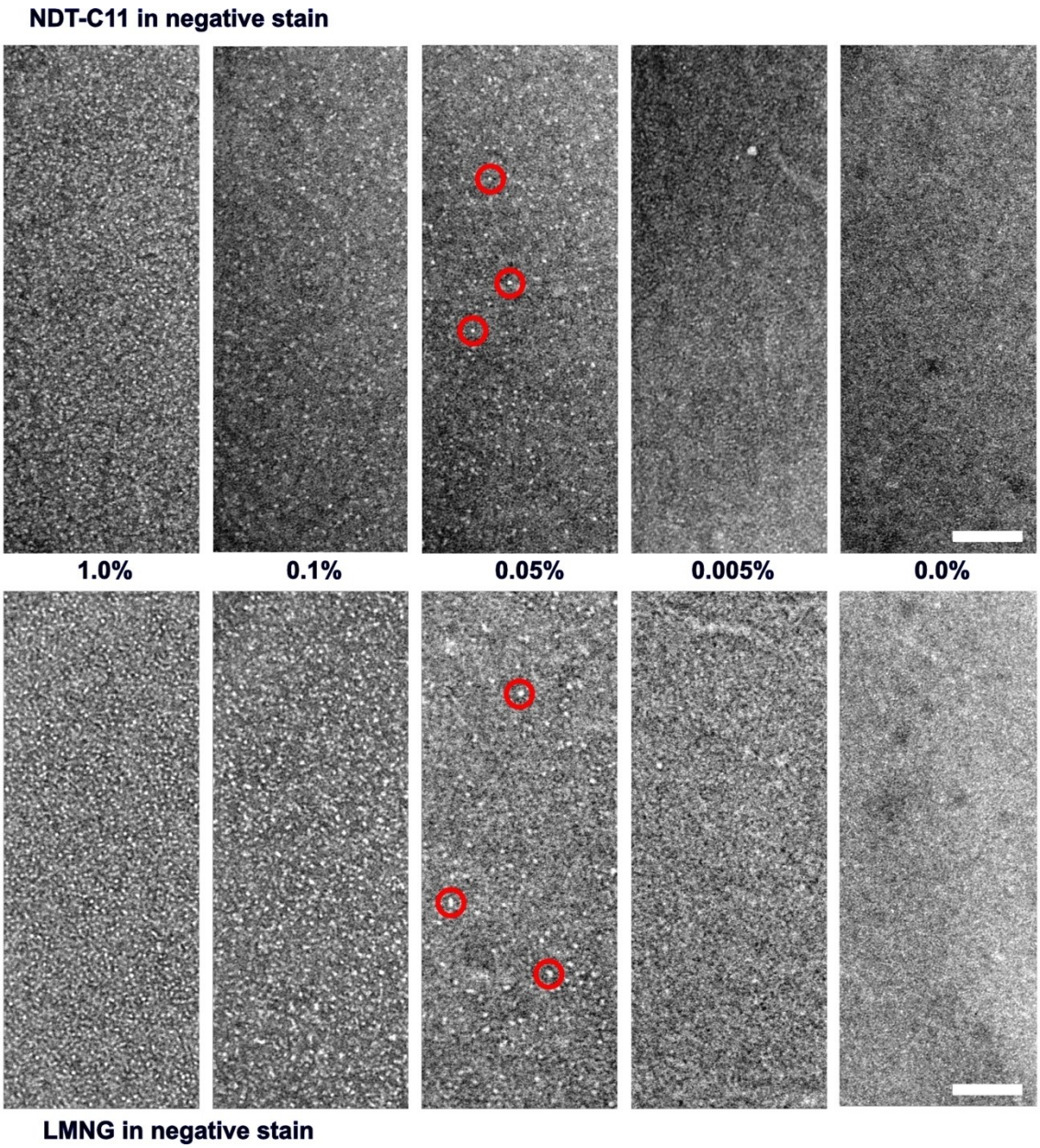


**Figure 3.** Representative transmission electron microscopy images of uranyl acetate-stained NDT-C11 and LMNG solubilized in a buffer of 30 mM Tricine-NaOH pH 8.0 and 75 mM NaCl at a concentration of 1.0%, 0.1%, 0.05%, 0.005% and 0.0% (w/w). Three NDT-C11 and LMNG detergent micelles are encircled in red. Note the absence of tubular micelles for 1% LMNG for the uranyl acetate stained solution. Scale bar 100 nm.

metry the NDT-C11 stabilized PSI solution was diluted 400 times in a detergent free buffer, with the expectation that the high affinity PDC of NDT-C11 bound to PSI would not lead to aggregation as a consequence of removing free detergent micelles. The measurements indicated good monodispersity (Figure 5a; Supplementary movie 1) of trimeric PSI, as well as the presence of small amounts of monomeric PSI and free NDT-C11 micelles. The calculated molecular size for all three peaks was well within the range expected for trimeric PSI, monomeric PSI and free detergent micelles of NDT-C11 (Figure 5b). Mass photometry was also performed on PSI trimer obtained using an SDG run in the presence of 0.05% DDM. As expected, dilution of DDM stabilized PSI complexes using a detergent free buffer did not allow interpretable measurements (Supplementary movie 2). These results suggest that NDT-C11 is a detergent highly compatible with characterization of IMPs by mass photometry.

In line with the results obtained by mass photometry, when performing negative stain EM on NDT-C11 PSI trimers, good monodispersity and the virtual absence of free detergent micelles was observed (Figure 4b). In conclusion, trimeric PSI prepared in NDT-C11 appeared to be well suited for cryo-grid vitrification. For a fair comparison of the behavior of trimeric PSI in either LMNG or NDT-C11 during cryo-grid vitrification, we froze cryo-grids using an identical purification batch and the same cryo-grid vitrification conditions with the only difference

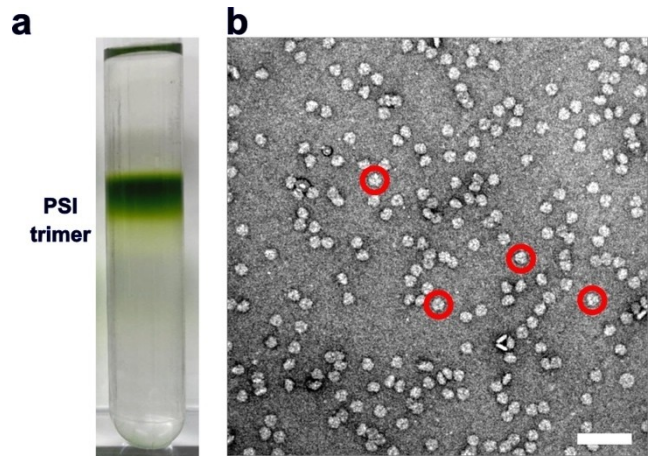


**Figure 4.** Photosystem I (PSI) detergent exchange to NDT-C11 and removal of excess free detergent via sucrose density gradient (SDG) ultracentrifugation. (a) Resulting gradient run at 0.005 % (w/w) NDT-C11. (b) Negative stained PSI trimer complexes from the recovered PSI trimer SDG fractions after removal of sucrose with four trimer complexes in top-view encircled in red. Scale bar 100 nm.

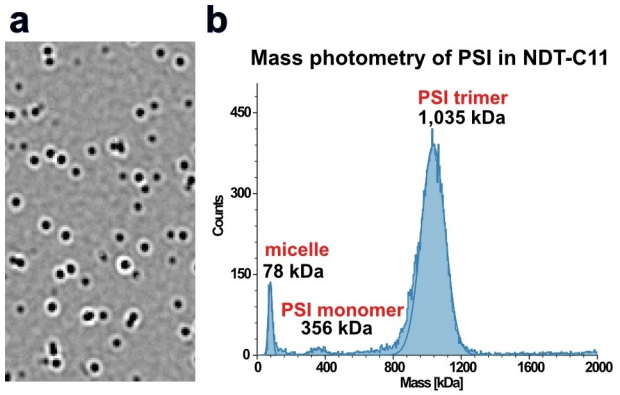


**Figure 5.** Mass photometry of the NDT-C11 SDG recovered PSI trimer fractions after sucrose removal and concentration. (a) Representative frame of the movie used for calculation of counting events displaying good monodispersity. (b) Peaks corresponding to the mass of the PSI trimer (theoretical MW 1,080 kDa), the PSI monomer (theoretical MW 360 kDa) and NDT-C11 micelles.

being the detergent used in the final SDG of the purification. As could be expected considering our previous experience with the *T. elongatus* PSI monomer and the PSI-LHCI complex from *Chlamydomonas reinhardtii*, PSI trimer complexes stabilized in LMNG exhibited a relatively strong tendency for small scale aggregation after cryo-grid vitrification (Figure 6a). In striking contrast, cryo-grids prepared with PSI trimer complexes stabilized in NDT-C11 did not exhibit any aggregation and particles appeared to be evenly dispersed and randomly orientated (Figure 6b).

This impression was confirmed by reference free 2D classification showing clear side, oblique and top views (Figure 6c). These results strongly suggest that NDT-C11 might be a very good choice for single particle cryo-EM structure determination of IMPs in general and in particular for photosystems. Since many single particle cryo-EM projects aimed at IMP structure determination are limited by suboptimal particle dispersion or preferred particle orientation, NDT-C11 is likely to be a valuable addition to the single particle cryo-EM toolbox. As a note of caution, we would like to point out that distribution of particle orientation for a given complex is dependent on many different factors and not buffer conditions alone. For example, in two previous studies GDN was used as the vitrification detergent for both PSI monomer and trimer, however, a strongly biased particle orientation distribution was observed only for the PSI monomer, but not for the trimer.[35,37] The biased orientation for the PSI monomer possibly was the consequence of particle crowding.

## NDT-C11 and Bovine F-ATP Synthase

Mammalian mitochondrial F-ATP synthase is a rotary molecular machine interconverting electrochemical energy in the form of the inner membrane proton motive force (pmf) and chemical energy in the form of a high ATP to ADP + Pi ratio.[41,42] The fragility of this 29 subunit membrane protein complex and its oligomeric organization into multimers of dimers along the ridge of mitochondrial cristae pose significant challenges for structural analysis by both X-ray crystallography and single particle cryo-EM, and until very recently reliable atomic models of the intact supercomplex were not available.[29,43] The situation improved dramatically with advances in single particle cryo-EM and the adoption of the novel lipid-like detergents LMNG and GDN for complex purification and cryo-grid vitrification – leading to reasonable atomic models for mammalian F-ATP synthase.[44–46] Still, structural analysis of the membrane spanning $F_o$ domain remains far from what has been achieved for PSI and the determination of dimer and higher oligomer structures is an open task. In its physiological environment of the inner mitochondrial membrane, mammalian F-ATP synthase is present as monomers, dimers and rows of dimers of varying length.[47,48] After membrane solubilization, however, its oligomeric state *in vitro* is highly dependent on buffer conditions and in particular the type and concentration of detergent used for complex stabilization.[28,49] Namely, while LMNG has been shown to favor monomer stabilization at higher detergent concentration, only digitonin and GDN proved sufficiently mild enough to stabilize dimers and higher oligomers in larger quantities.[28,29,45–47] Recently, we reported that monomeric bovine F-ATP synthase can be obtained from GDN-isolated oligomeric F-ATP synthase by a brief pre-incubation in 0.5 % LMNG and a subsequent sucrose density gradient (SDG) ultracentrifugation step in 0.02 % LMNG.[28] To probe the level of mildness NDT-C11 has in comparison to GDN and LMNG we conducted the above described bovine F-ATP synthase monomer isolation procedures on the same batch of GDN-stabilized oligomeric F-ATP synthase, however, using either LMNG or NDT-C11 for the pre-incubation and the final sucrose density gradient (Figure 7a).

Analysis of gradient fractions by clear native-PAGE (CN-PAGE) did not indicate the presence of any lower molecular weight proteins, underlining the high stability of bovine F-ATP

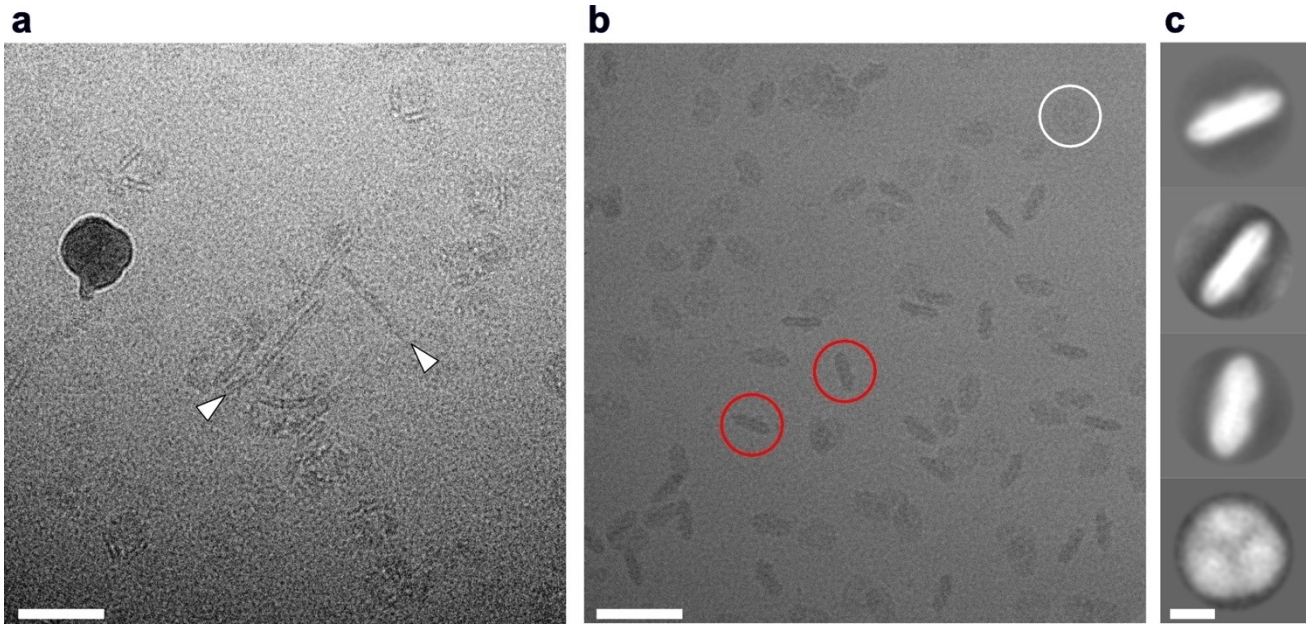


**Figure 6.** Cryo-EM of LMNG and NDT-C11 stabilized PSI trimer. (a) Typical image of LMNG stabilized PSI trimers. Row-like particle aggregation of several complexes indicative of suboptimal dispersion in LMNG are marked by white triangles. Scale bar 50 nm. (b) Typical image of NDT-C11 stabilized trimers. Well dispersed particles can be seen in the whole field of view. Two side views are encircled in red and a top view in white. Scale bar 50 nm. (c) 2D classes of PSI trimer stabilized in NDT-C11 showing side-views, oblique-views and top-views. Scale bar 10 nm.

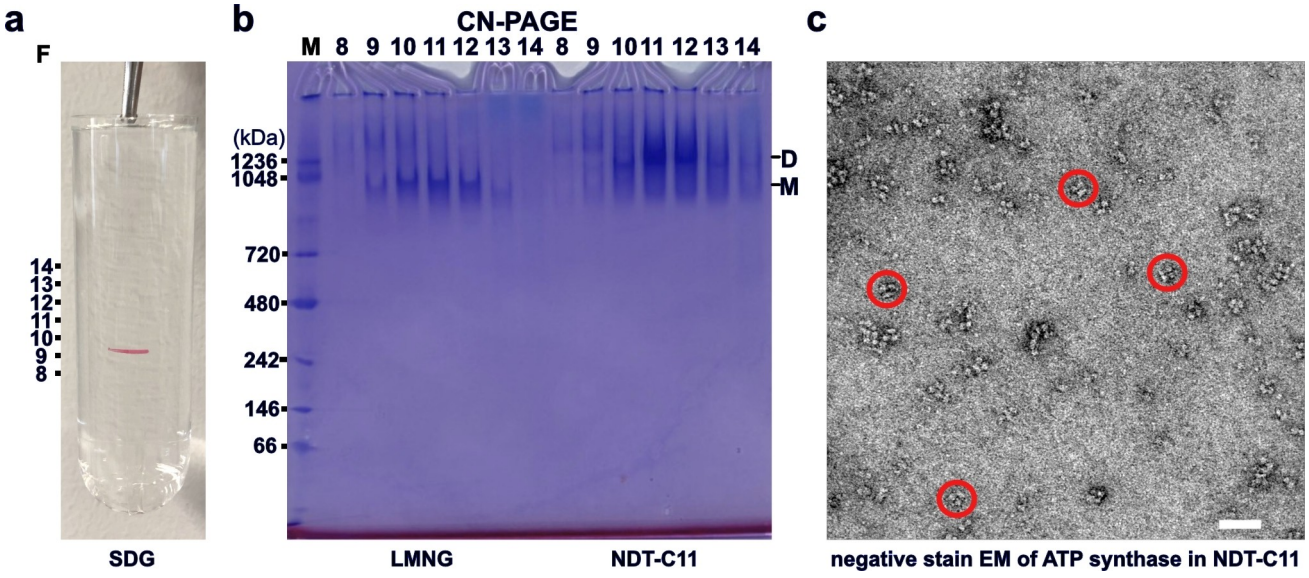


**Figure 7.** Bovine F-ATP synthase detergent exchange to NDT-C11 and removal of excess free detergent via sucrose density gradient (SDG) ultracentrifugation. (a) The resulting SDG run at 0.02% (w/w) NDT-C11 with positions of fractions used for the subsequent analysis by CN-PAGE indicated. (b) Clear native PAGE of sucrose gradient fractions run in either 0.02% LMNG or NDT-C11. Native molecular weight marker (M) are indicated in kDa and the positions of monomer and dimer bands are indicated by M and D, respectively. (c) Negative stain EM of NDT-C11 fraction 11 after sucrose removal and 30x dilution. Some apparently dimeric complexes are encircled in red. Scale bar 50 nm.

synthase in both LMNG and NDT-C11. Bands from NDT-C11 fractions were shifted to higher molecular weight in comparison to that of LMNG-treated oligomers (Figure 7b). This indicates that while NDT-C11-treated oligomers were not preserved, NDT-C11 did not fully monomerize the F-ATP synthase oligomer fraction, suggesting that NDT-C11 is milder than LMNG, but harsher than GDN in terms of preserving mammalian F-ATP synthase oligomer contacts. Examination of NDT-C11 gradient fractions by negative stain EM showed a reasonable level of monodispersity and apparently a larger number of dimeric complexes, an observation that is in line with the observed up-shift of bands relative to monomeric F-ATP synthase in CN-PAGE gels (Figure 7c).

To further examine if NDT-C11 stabilized F-ATP synthase complexes behave differently from LMNG-stabilized complexes during cryo-grid vitrification, we performed cryo-EM imaging.

For vitrification, standard holey carbon grids and standard blotting conditions were used in identical fashion on both samples. Examination of the resulting cryo-grids did show a poor level of particle dispersion for both NDT-C11 and LMNG stabilized F-ATP synthase that had no obvious positive difference for the former (Supp. Figure 2a,b). Thus, unlike for trimeric PSI, switching the vitrification detergent alone did not improve particle dispersion. However, when we changed grid type and blotting conditions slightly (300 mesh to 200 mesh, 3 s blotting to 2 s blotting), we could observe a difference in particle dispersion with NDT-C11 stabilized F-ATP synthase exhibiting better particle dispersion (Figure 8a,b). This indicates that for overcoming problems in particle dispersion NDT-C11 might be very useful for some projects, but that it is not a 'magic bullet' that can promote good particle dispersion during cryo-grid vitrification for all IMPs in a similar fashion.

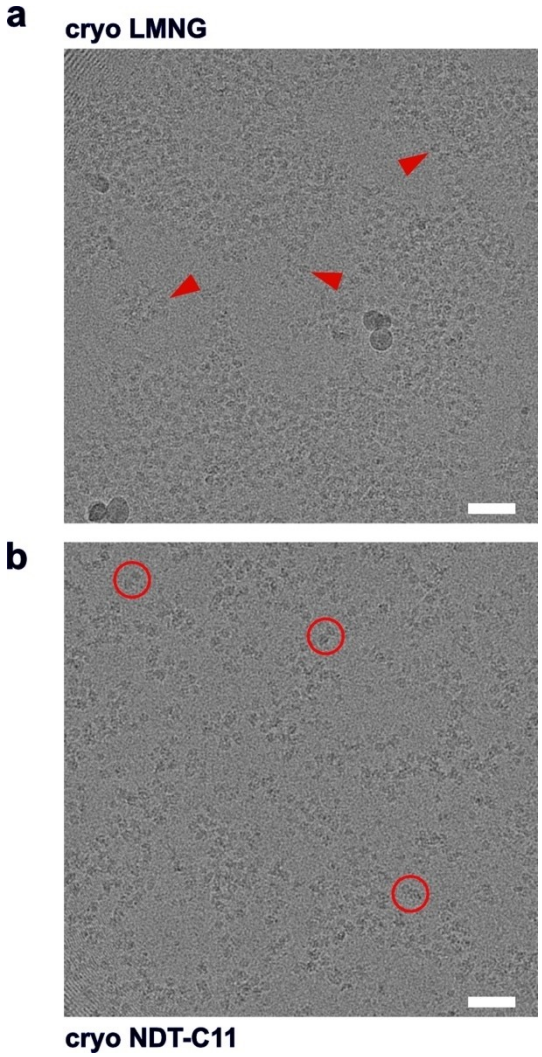


**Figure 8.** Cryo-images of bovine F-ATP synthase stabilized in either LMNG or NDT-C11. (a) Representative cryo-image of bovine F-ATP synthase after exchange to LMNG and removal of sucrose. Three F-ATP synthase particles are indicated by red triangles. Scale bar 50 nm. (b) Representative cryo-image of bovine F-ATP synthase after exchange to NDT-C11 and removal of sucrose. Three F-ATP synthase particles are encircled in red. Scale bar 50 nm.

Single particle cryo-EM has now emerged as the dominant method for the experimental structure determination of integral membrane proteins.[3,50,51] Though this is only a recent trend, it is expected that this trend will continue and even speed up with the ongoing popularization and development of cryo-EM. Even though membrane mimetics such as amphipols, SMALPs, nano-discs and liposomes are popular, the majority of IMP single particle cryo-EM is still done with the help of small amphiphiles – detergents. The relatively novel lipid-like detergents LMNG and GDN, introduced 14 and 12 years ago, have enjoyed great success in their application to single particle cryo-EM. They were, however, originally developed as new tools for X-ray crystallography and not for single particle cryo-EM. This circumstance underlines that the field could benefit immensely from the development of novel detergents that are specifically tailored to the needs of single particle cryo-EM.

With NDT-C11 being a headgroup and linker region derivate of LMNG, there is a good chance that NDT-C11 outperforms LMNG as a detergent for single particle cryo-EM. This assumption was the motivation for the here reported study and has been strengthened in this first preliminary survey of NDT-C11 properties in its use for single particle cryo-EM. We believe that the headgroup and linker region modifications present valuable, unharnessed opportunities for single particle cryo-EM going beyond improved stability of fragile membrane complexes and potentially alleviating common challenges in particle dispersion and preferred orientation. Given the success of LMNG and GDN in their use as membrane mimetics in cryo-grid vitrification, we speculate that their lipid-like tail region conveys favorable properties, while headgroup derivates that result in more compact headgroup regions of the PDC might be a future direction for further improvements. Similarly, specific tailoring of detergent design might also boost the usability of auto-insertion as a mild technique for the production of proteoliposomes for cryo-EM imaging of membrane proteins under close to physiological, non-equilibrium conditions.[52] In this respect, the very recent introduction of a linker region capable of mediating hydrogen bonds in the novel detergent class of melamine-cored glucosides is very exciting.[53] Potentially the changed PDC properties might be better at mimicking the lateral pressure profile of the lipid bilayer and perhaps a very compact PDC could promote higher stability at the air-water interface, improve particle dispersion and boosting random orientation distribution.

Recent advances in cryo-EM have made it possible to obtain good structures of IMPs without the need to solubilize cellular membranes and purify target complexes. This was achieved by either *in situ* imaging of cryo-focused ion beam milled cells[54,55] or the imaging of small vesicles derived from cells expressing the target complex.[56,57] In addition, the recent release of AlphaFold3 is a game changer in respect to *in silico* investigation of protein-protein and protein-ligand interaction, enabling predictions of environmental influence on protein structure that can match the best experimental results.[58] The above raises the question, if *in vitro* structural analysis of purified IMPs will become obsolete. We do not think so. For many types of structural investigations, obtaining high resolu-

tion structures under strictly controlled *in vitro* conditions is crucial, which is harder to achieve when using cell derived small vesicles and clearly out of reach for *in situ* structures. Protein complex dynamics is another realm of structural analysis that will be hard to tackle by either *in situ* or *in silico* investigation. In addition, as demonstrated in a recent study on structure based drug development of an gastric H,K-ATPase acid blocker,[59] speed can be key too. In that study, rapid structure determination at high resolution (2.26–2.08 Å) provided a feedback loop on exact novel compounds binding poses which was crucial to drive the project forward. This speedy feedback loop was made possible by single particle cryo-EM of detergent solubilized H,K-ATPase.

## Conclusions

In this study, we examined the potential usefulness of the novel detergent NDT-C11 in single particle cryo-EM in comparison to the established and popular detergent LMNG. Even at higher detergent concentration no tendency for the formation of elongated free detergent micelles could be observed for NDT-C11, a tendency that is a major drawback of LMNG. In agreement with its reported low CMC and high affinity for integral membrane proteins, removal of free detergent micelles by sucrose density gradient ultracentrifugation did not cause aggregation nor precipitation in both *T. elongatus* PSI and bovine F-ATP synthase. In terms of mildness, NDT-C11 appeared to be better than LMNG, but worse than GDN in preserving oligomer contacts in bovine F-ATP synthase. Particle dispersion after cryo-grid vitrification was greatly improved for PSI and slightly improved for F-ATP synthase. In addition, particle orientation is potentially less prone to be preferential for NDT-C11 stabilized complexes. In summary, NDT-C11 is a very promising novel detergent that has the potential to replace LMNG as a major tool for high resolution single particle cryo-EM of fragile membrane proteins. Therefore, NDT-C11 clearly deserves wider testing by the community. For that to occur, commercialization of NDT-C11 is mandatory and hopefully its straightforward four step synthesis will alleviate another major drawback of LMNG – its price.

## Experimental Section

### Materials and Chemicals

Materials and chemicals were all obtained commercially and used as received with the exception of NDT-C11, which was synthesized in the Chae lab as previously described.[30] $^{1}$H and $^{13}$C NMR spectra of this detergent obtained from the Chae lab were the same as those described in the original report. $^{1}$H NMR (400 MHz, MeOD): $\delta$ 4.31 (d, $J$=7.8 Hz, 3H), 3.98 (d, $J$=10.0 Hz, 3H), 3.85 (dd, $J$=12.0, 2.0 Hz, 3H), 3.69–3.62 (m, 6H), 3.48 (s, 2H), 3.37–3.25 (m, 10H), 3.19 (t, $J$=8.4 Hz, 3H), 1.56–1.50 (m, 1H), 1.38–1.20 (m, 40H), 0.90 (t, $J$=6.9 Hz, 6H); $^{13}$C NMR (101 MHz, MeOD): $\delta$ 105.2, 78.1, 77.9, 76.0, 75.2, 71.7, 70.7, 70.1, 62.8, 46.7, 39.4, 33.1, 32.6, 31.2, 30.9, 30.5, 28.0, 23.8, 14.5.

### Purification of Trimeric Photosystem I

Trimeric PSI was purified from cultured *T. elongatus* cells as previously described[35] with exception of using either LMNG or NDT-C11 for the final sucrose density gradient. In brief, Thermophilic cyanobacteria of the Synechocystis sp. PCC 6803 mutant strain, genetically modified with an N-terminal His10-tag on the PsaF subunit as well as a chloramphenicol-resistant gene as a selectable marker, were cultivated under illumination for the purification of PSI trimers. Cultivation was performed under continuous illumination at 30 μM photons $m^{-2}$ $s^{-1}$ at 50 °C in BG11 medium. A total of 16 L culture solution was harvested when the OD730 nm absorbance reached 1.0. Harvested cells were concentrated by centrifugation (8,000 g, 2 min at 4 °C, JLA 9.1000 rotor, Avanti™ HP-26XP), re-suspended in Buffer A (75 mM NaCl and 30 mM Tricine-NaOH at pH 8.0) and then frozen by liquid nitrogen for storage at −80 °C or used immediately for cell disruption by the beads-beating method. Cells were disrupted in freshly prepared pre-cooled Buffer B (same components as in Buffer A with the addition of 1 mM Benzamidine, 1 mM 6-aminohexanoic acid, 1 mM PMSF solubilized in ethanol, and 1 mM DNase I) and thylakoid membranes were separated from soluble cellular contents by ultracentrifugation (40,000 g, 30 min at 4 °C, P50AT2 rotor, HITACHI himac CP80WX). Thylakoid membranes were re-suspended in Buffer A at a chlorophyll concentration of 1 mg/mL, and subsequently a 10% β-DDM stock solution was added dropwise until the concentration of β-DDM in buffer reached 1%. Then the mixture was incubated in the dark at 4 °C with gentle stirring for 45 min. After membrane solubilization, insoluble contents were removed by ultracentrifugation (50,000 g, 30 min at 4 °C, P50AT2 rotor, HITACHI himac CP80WX) and the supernatant was applied directly to the sucrose density gradient, as well as to an open column with Ni-NTA Sepharose (Qiagen). PSI trimers were eluted from the column using Buffer C (75 mM NaCl, 30 mM Tricine-NaOH at pH 8.0, 0.05% β-DDM and 100 mM imidazole). Eluted PSI trimers were concentrated by ultrafiltration (Amicon15 ultrafiltration tubes, 100 kDa MWCO at 3,000 g and 4 °C) to a final chlorophyll concentration of ~10 mg/mL. The chlorophyll concentration (Cchl) was measured by a spectrophotometer (U5100, Hitachi) based on previous protocol. For PSI-related samples, chlorophyll concentration was determined by measuring absorbance at wavelength of 663 nm (A663) in 80% acetone as Cchl (mg/mL) = 12.17×A663. Based on the chlorophyll molecular weight ratio in PSI, the PSI protein concentration (Cpro) could be calculated as Cpro (mg/mL) = Cchl×3.92. The step gradient buffer for SDG was prepared containing 75 mM NaCl, 30 mM Tricine-NaOH at pH 8.0, 0.05% β-DDM and sucrose concentration were 40% (w/v), 30%, 20% and 10% from centrifuge tube bottom to top respectively. Step gradient buffers were applied at the top of Ultra-Clear™ centrifuge tubes (Beckman Coulter™) gently using a 5 mL pipette in sequence from highest sucrose (bottom) to lowest (top). The total volume for each tube was 30 mL (7.5 mL for each step buffer). Gradient buffer mixture should be prepared before use (within 3 hours), and maximum 1 mL concentrated PSI sample could be loaded at top of each tube. Centrifugation was performed at 4 °C with speed of 20,000 g for 20 hours (P28S rotor, HITACHI himac CP80WX). After centrifugation, each separated bounds were extracted carefully in sequence from top to bottom. After sample extraction of separated bands as described above, the second-round SDG was performed for detergent exchange. Continues sucrose gradients were prepared using a Gradient Master™107 (Biocomp). The total volume for each tube was 10 mL (5 mL each for the buffer containing 40% and 10% sucrose). The gradient buffer contains 75 mM NaCl, 30 mM Tricine-NaOH at pH 8.0 in 0.005% LMNG or 0.005% NDT-3.

Centrifugation was performed at 4 °C with speed of 20,000 g for 20 hours (P40ST rotor, HITACHI himac CP80WX). PSI trimers from the corresponding band were collected, and a desalting column (PD-10, GE Healthcare, Chicago, IL, USA) was used for removing sucrose and for buffer exchange. Final PSI trimers were concentrated to a chlorophyll concentration of 10 mg/mL in buffer D (10 mM Tricine, pH 8.0, 10 mM $MgCl_2$, and 0.005% LMNG or NDT-C11) and examined for purity, stability, and monodispersity using negative stain electron microscopy as described below. The final PSI trimer sample was flash frozen in liquid nitrogen in 10 μL aliquots using photophobic EP tubes and stored until further use at −80 °C. Protein concentration of PSI trimer was determined based on the chlorophyll content ratio of CPro/CChl = 3.92.

### Purification of Bovine F-ATP Synthase

F-ATP synthase was purified from bovine heart muscle tissue mitochondria as previously described[28] except that for detergent exchange pre-incubation and a final sucrose density gradient step either LMNG or NDT-C11 were employed. In brief, a single bovine heart was obtained from a local abattoir immediately after animal sacrifice. Fat tissue was removed and 600 g of lean, red meat minced using a commercial meat mincer. The mince is placed into 2.3 L of ice-cold distilled water supplied with 350 ml of ice-cold phosphate buffer (0.2 M NaPi, pH 7.4), and a spate of PMSF. This mixture is homogenized in a Polytron PT3100D homogenizer at 11,000 rpm for 10 min. Larger cell debris is removed by spin-down at 2800 rpm for 20 min at 4 °C with a large-scale refrigerated centrifuge (Hitachi Himac CR20G) using a R2A rotor. Subsequently, the supernatant is carefully separated from the soft pellet by straining through two sheets of gauze. Thereafter, mitochondria are pelleted from the strained supernatant by centrifugation at 8000 rpm for 25 min at 4 °C with a large- scale refrigerated centrifuge (Hitachi Himac CR20G) using a R12A F rotor and the supernatant is discarded. The mitochondrial precipitate is suspended in a buffer of 40 mM HEPES-NaOH (pH 7.3), 5 mM $MgCl_2$, 5 mM DTT, 5 mM EGTA, and 0.5 mM ADP and homogenized using a loosely fitting Dounce glass homogenizer by 12 up-down movements. From the resulting homogenate, the inner mitochondrial membrane fraction is pelleted by ultracentrifugation for 30 min at 100,000 g using a Hitachi Himac CP80WX ultracentrifuge with a P45A T-angle rotor. After discarding the resulting supernatant by aspiration and careful wiping of residual oil from the ultracentrifuge tubes, the total amount of inner mitochondrial membrane is weighted for later adjustment of the membrane-to-detergent ratio. Pellets of inner mitochondrial membrane are suspended in a buffer of 40 mM HEPES-NaOH (pH 7.3), 5 mM $MgCl_2$, 5 mM DTT, 5 mM EGTA, and 0.5 mM ADP at a volume to weight ratio of 1 L buffer to 560 g membranes. The suspension is homogenized by approximately 12 up-down movements in a tightly fitting glass Dounce homogenizer to obtain inside-out vesicles. Note that the resulting pH of the homogenate will be slightly acidic. Solubilization of the inside-out membrane fraction is performed under constant magnetic stirrer mixing at ice- cold temperature. First, sodium deoxycholate is added to a final concentration of 0.73% (w/v) from an 11% stock solution, second, DM is added to a final concentration of 0.4% (w/v) from a 20% stock solution, after which solid KCl is added to a final concentration of 72 g/l. Finally, when the KCl salt grains are completely dissolved, GDN is added to a final concentration of 0.1% (w/v). To remove insolubilized membranes the solution is ultracentrifuged for 40 min at 176,000 g using a Hitachi P45A T-angle rotor. The resulting supernatant is strained through four layers of gauze and kept for equilibrium ultracentrifugation. A two-step sucrose gradient is prepared in large fixed angle rotor ultracentrifuge tubes using 16 ml of 2.3 M sucrose and 24 ml 1.6 M sucrose solubilized in a buffer of 40 mM HEPES-NaOH (pH 7.3), 5 mM $MgCl_2$, 5 mM DTT, 5 mM EGTA, 0.5 mM ADP, 100 mM KCl, 0.1% DM (w/v), 0.02% GDN, and 0.02% LMNG. The solubilized inside-out vesicle solution is gently layered onto the two-step sucrose gradient and ultra- centrifuged to equilibrium at 176,000 g for 42 h at 4 °C using a Hitachi P45A T-angle rotor. The resulting gradient is collected in 2 ml fractions from the bottom of each ultracentrifuge tube using a peristaltic pump and fractions are examined for enrichment of F-ATP synthase with low ATP hydrolysis activity using a combination of SDS-PAGE, CN-PAGE, and the Pullman ATP hydrolysis activity assay. Fractions containing a high concentration of F-ATP synthase, but exhibiting relatively low ATP hydrolysis activity are pooled and diluted in a buffer of 40 mM HEPES-NaOH (pH 7.3), 5 mM $MgCl_2$, 5 mM DTT, 5 mM EGTA, 0.5 mM ADP, 100 mM KCl, and 0.02% GDN to a final sucrose concentration that is slightly below 0.6 M sucrose as monitored using a PAL-1 pocket refractometer (Atago). A step gradient of sucrose solution is layered into large ultracentrifuge tubes from bottom-to-top using 10 ml of 1.6 M, 10 ml of 1.0 and 10 ml of 0.6 M sucrose solution with all solution prepared using a buffer of 40 mM HEPES-NaOH (pH 7.3), 5 mM $MgCl_2$, 5 mM DTT, 5 mM EGTA, 0.5 mM ADP, 80 mM KCl, and 0.02% GDN. The pooled and diluted F-ATP synthase fractions are gently layered onto the step gradient and ultra- centrifuged at 176,000 g for 20 h at 4 °C using a Hitachi P45A T- angle rotor. The resulting gradient is collected in 2 ml fractions from the bottom of each ultra-centrifuge tube using a peristaltic pump, and fractions are examined for enrichment of F-ATP synthase by SDS-PAGE and CN-PAGE. Fractions enriched in F-ATP synthase are pooled and diluted to 19% sucrose as monitored using a PAL-1 pocket refractometer (Atago) in a buffer of 40 mM HEPES-NaOH (pH 7.3), 5 mM $MgCl_2$, 5 mM DTT, 5 mM EGTA, 0.5 mM ADP, 100 mM KCl, and 0.02% GDN. Using a Gradient Master 108, Biocomp a continuous 40 to 20% sucrose gradient is prepared in swing-out rotor tubes (Open-Top Thinwall Ultra-Clear Tube, 25×89 mm) with a buffer composition of 40 mM HEPES-NaOH (pH 7.3), 5 mM $MgCl_2$, 5 mM DTT, 5 mM EGTA, 0.5 mM ADP, 100 mM KCl, and 0.02% of either LMNG or NDT-C11. The pooled and diluted F-ATP synthase fractions are supplemented with either LMNG or NDT-C11 to a final concentration of 0.5% (w/v) and incubated for 2 h. Subsequently, the solution is gently layered onto the gradient and ultracentrifuged at 113,000 g for 20 h using a swing-out rotor P28S (Hitachi). The resulting gradient is collected in 2 ml fractions from the bottom of each ultracentrifuge tube using a peristaltic pump and fractions are examined for enrichment of monomeric F-ATP synthase by SDS-PAGE, CN-PAGE, and negative stain EM.

### Clear Native Gel Electrophoresis

Typically, 4 μl of sample was applied to gel pockets and native gel electrophoresis performed at 4 °C using 3 to 12% Bis-Tris gels from Invitrogen and native running buffers from SERVA running at 150 CV for 90 min. As a molecular weight marker, NativeMark Unstained Protein Standard (Invitrogen) was used in all clear native gel electrophoresis experiments. Gels were stained by SERVA Blue R staining kit (Serva).

### Negative Stain EM

An aliquot of 3.0 μl of enriched fraction was diluted x100 and applied to glow-discharged (5 mA, 10 s, Eiko LifeSciences)

continuous carbon film coated copper grids (Nisshin EM). Staining was performed by applying 3.0 μl 2% uranyl acetate solution. After incubation for 30 s, staining solution was blotted using filter paper (Whatman #1; Whatman) and air dried. Specimen was inspected using a H-7650 HITACHI trans- mission electron microscope at 80 kV acceleration voltage equipped with a 1×1K Tietz FastScan- F114 CCD camera.

### Cryo-EM

Sample was applied to a freshly glow-discharged (10 s, 10 mA at 7 Pa using a JEOL JEC-3000FC) Quantifoil holey carbon grid (R1.2/1.3, Cu, 300 mesh) using a Vitrobot Mark IV (FEI) at 8 °C with a blotting time of 3 s at blot force 10 and 100% humidity for plunge-freezing into liquid ethane. For bovine F-ATP synthase as a second cryo-grid preparation condition LMNG or NDT-C11 stabilized sample was applied to a freshly glow-discharged (10 s, 10 mA at 7 Pa using a JEOL JEC-3000FC) Quantifoil holey carbon grid (R1.2/1.3, Cu, 200 mesh) using a Vitrobot Mark IV (FEI) at 8 °C with a blotting time of 2 s at blot force 15 and 100% humidity for plunge-freezing into liquid ethane. The prepared grids were either transferred to a CRYO ARM 300 (JEOL) transmission cryo electron microscope (EM01CT at SPring-8) running at 300 kV and equipped with an Omega-type in-column energy filter and a Gatan K3 camera in correlated-double sampling mode, counting mode or to to a CRYO ARM 200 (JEOL) transmission cryo electron microscope (EM02CT at SPring-8) running at 200 kV and equipped with an Omega-type in-column energy filter and a Gatan K2 camera in counting mode or a Glacios (Thermo Fisher Scientific) trans-mission cryo electron microscope (EM04CT at SPring-8) running at 200 kV with a Falcon4i in counting mode. Imaging was performed using either JADAS (JEOL) or SerialEM,[60] including yoneoLocr[61] integrated as a SerialEM macro for hole centering, at a nominal magnification of 60,000×, corresponding to a calibrated pixel size of 0.752 Å/pix (EM01CT at SPring-8) or 0.849 Å/pix (EM02CT at SPring-8) or, at a nominal magnification of 110,000x, corresponding to a calibrated pixel size of 1.2 Å/pix (EM04CT at SPring-8). Image processing was done in RELION 4.1.[62]

### Mass Photometry

The MP experiments were performed at room temperature using the RefeynTwo instrument (Refeyn, Oxford, UK) following the standard protocol. A 2 min video was recorded using the AcquireMP (Refeyn, Oxford, UK) software. The MP video files were processed using the DiscoverMP software (Refeyn, Oxford, UK), as previously described.

### ATPase Activity Assay

The ATPase activity of purified F-ATP synthase was measured at room temperature using a NADH-coupled assay. The assay mixtures contained 40 mM K·Pi (pH 7.8), 150 mM KCl, 2 mM $MgCl_2$, 2.5 mM phosphoenolpyruvate, 100 μg/ml pyruvate kinase, 100 μg/ml lactate dehydrogenase, and 0.2 mM NADH, and 2.5 mM ATP·$Mg^{2+}$. The reaction was initiated by adding 0.01 mg of F-ATP synthase fraction to 2 ml of the reaction mixture. The hydrolysis of ATP by the F-ATP synthase was followed by NADH oxidation at 340 nm at 20 °C.

## Supporting Information

Two movies and three figures are included as supporting information.

## Acknowledgements

We would like to thank Masaki Yamamoto for his support throughout the project. This work was funded by JSPS grant 20J40167 and 19K15749 (C. J.); the Naito Foundation Subsidy for Female Researchers after Maternity Leave (C. J.); a BINDS grant from AMED (JP24ama121001 to Masaki Yamamoto and C. G.) and the JST-CREST under grant number JPMJCR20E1 (G. K.).

## Conflict of Interests

The authors declare no conflict of interest.

## Data Availability Statement

The data that support the findings of this study are available from the corresponding author upon reasonable request.

**Keywords:** cryoEM · detergent · membrane protein · vitrification · single particle analysis

[1] C. Gerle, *J. Membr. Biol.* **2019**, *252*, 115–130, DOI 10.1007/s00232-019-00061-w.
[2] S. J. Singer, G. L. Nicolson, *Sci. (New York, NY)* **1972**, *175*, 720–731.
[3] C. Le Bon, B. Michon, J. L. Popot, M. Zoonens, *Q. Rev. Biophys.* **2021**, *54*, 1–22, DOI 10.1017/S0033583521000044.
[4] R. Santos, O. Ursu, A. Gaulton, A. P. Bento, R. S. Donadi, C. G. Bologa, A. Karlsson, B. Al-Lazikani, A. Hersey, T. I. Oprea, J. P. Overington, *Nat. Rev. Drug Discovery* **2016**, *16*, 19–34.
[5] R. M. Bill, P. J. Henderson, S. Iwata, E. R. Kunji, H. Michel, R. Neutze, S. Newstead, B. Poolman, C. G. Tate, H. Vogel, *Nat. Biotechnol.* **2011**, *29*, 335–340.
[6] S. K. Burley, H. M. Berman, C. Bhikadiya, C. Bi, L. Chen, L. Di Costanzo, C. Christie, J. M. Duarte, S. Dutta, Z. Feng, S. Ghosh, D. S. Goodsell, R. K. Green, V. Guranovic, D. Guzenko, B. P. Hudson, Y. Liang, R. Lowe, E. Peisach, I. Periskova, C. Randle, A. Rose, M. Sekharan, C. Shao, Y. P. Tao, Y. Valasatava, M. Voigt, J. Westbrook, J. Young, C. Zardecki, M. Zhuravleva, G. Kurisu, H. Nakamura, Y. Kengaku, H. Cho, J. Sato, J. Y. Kim, Y. Ikegawa, A. Nakagawa, R. Yamashita, T. Kudou, G. J. Bekker, H. Suzuki, T. Iwata, M. Yokochi, N. Kobayashi, T. Fujiwara, S. Velankar, G. J. Kleywegt, S. Anyango, D. R. Armstrong, J. M. Berrisford, M. J. Conroy, J. M. Dana, M. Deshpande, P. Gane, R. Gáborová, D. Gupta, A. Gutmanas, J. Koča, L. Mak, S. Mir, A. Mukhopadhyay, N. Nadzirin, S. Nair, A. Patwardhan, T. Paysan-Lafosse, L. Pravda, O. Salih, D. Sehnal, M. Varadi, R. Va˘reková, J. L. Markley, J. C. Hoch, P. R. Romero, K. Baskaran, D. Maziuk, E. L. Ulrich, J. R. Wedell, H. Yao, M. Livny, Y. E. Ioannidis, *Nucleic Acids Res.* **2019**, *47*, D520–D528.
[7] The Stephen White database of Membrane Proteins of Known 3D Structure can be found under: https://blanco.biomol.uci.edu/mpstruc, **1998** (accessed 20 May 2024).
[8] Y. Cheng, *Cell* **2015**, *161*, 450–457, DOI 10.1016/j.cell.2015.03.049.
[9] W. Kühlbrandt, *Science* **2014**, *343*, 1443–1444, DOI 10.1126/science.1251652.
[10] R. Danev, M. Belousoff, Y. L. Liang, X. Zhang, F. Eisenstein, D. Wootten, P. M. Sexton, *Nat. Commun.* **2021**, *12*, 1–10.

[11] R. Danev, H. Yanagisawa, M. Kikkawa, *Microscopy* **2021**, *70*, 487–497.
[12] A. Sadaf, K. H. Cho, B. Byrne, P. S. Chae, *Amphipathic Agents for Membrane Protein Study*, Elsevier Inc., **2015**.
[13] J. W. Young, *Biochem. Soc. Trans.* **2023**, *51*, 1405–1416.
[14] M. Woubshete, S. Cioccolo, B. Byrne, *ChemPlusChem* **2024**, *89*, 1–12, DOI 10.1002/cplu.202300678.
[15] H. J. Lee, H. S. Lee, T. Youn, B. Byrne, P. S. Chae, *Chem* **2022**, *8*, 980–1013.
[16] J. Deisenhofer, O. Epp, K. Miki, R. Huber, H. Michel, *Nature* **1985**, *318*, 618–624, DOI 10.1038/318618a0.
[17] C. Ostermeier, H. Michel, *Curr. Opin. Struct. Biol.* **1997**, *7*, 697–701.
[18] P. Rosevear, T. VanAken, J. Baxter, S. Ferguson-Miller, *Biochemistry* **1980**, *19*, 4108–4115.
[19] P. S. Chae, S. G. F. Rasmussen, R. R. Rana, K. Gotfryd, R. Chandra, M. A. Goren, A. C. Kruse, S. Nurva, C. J. Loland, Y. Pierre, D. Drew, J. L. Popot, D. Picot, B. G. Fox, L. Guan, U. Gether, B. Byrne, B. Kobilka, S. H. Gellman, *Nat. Methods* **2010**, *7*, 1003–1008.
[20] P. S. Chae, S. G. F. Rasmussen, R. R. Rana, K. Gotfryd, A. C. Kruse, A. Manglik, K. H. Cho, S. Nurva, U. Gether, L. Guan, C. J. Loland, B. Byrne, B. K. Kobilka, S. H. Gellman, *Chem. A Eur. J.* **2012**, *18*, 9485–9490.
[21] F. Hauer, C. Gerle, N. Fischer, A. Oshima, K. Shinzawa-Itoh, S. Shimada, K. Yokoyama, Y. Fujiyoshi, H. Stark, *Structure* **2015**, *23*, 1769–1775, DOI 10.1016/j.str.2015.06.029.
[22] H. Guo, S. A. Bueler, J. L. Rubinstein, *Science* **2017**, *358*, 936–940.
[23] C. Vénien-Bryan, C. A. H. Fernandes, *Int. J. Mol. Sci.* **2023**, *24*, 1–25, DOI 10.3390/ijms241914785.
[24] K. R. Vinothkumar, R. Henderson, *Q. Rev. Biophys.* **2016**, *49*, 1–25, DOI 10.1017/s0033583516000068.
[25] C. Breyton, W. Javed, A. Vermot, C. A. Arnaud, C. Hajjar, J. Dupuy, I. Petit-Hartlein, A. Le Roy, A. Martel, M. Thépaut, C. Orelle, J. M. Jault, F. Fieschi, L. Porcar, C. Ebel, *Biochim. Biophys. Acta Biomembr.* **2019**, *1861*, 939–957.
[26] C. Gerle, J. I. Kishikawa, T. Yamaguchi, A. Nakanishi, O. Çoruh, F. Makino, T. Miyata, A. Kawamoto, K. Yokoyama, K. Namba, G. Kurisu, T. Kato, *Microscopy* **2022**, *71*, 249–261.
[27] C. Jiko, K. M. Davies, K. Shinzawa-Itoh, K. Tani, S. Maeda, D. J. Mills, T. Tsukihara, Y. Fujiyoshi, W. Kühlbrandt, C. Gerle, *eLife* **2024**, *4*, e06119. DOI 10.7554/eLife.06119.001.
[28] C. Jiko, Y. Morimoto, T. Tsukihara, C. Gerle, *J. Biol. Chem.* **2024**, *300*, 105603.
[29] J. Gu, L. Zhang, S. Zong, R. Guo, T. Liu, J. Yi, P. Wang, W. Zhuo, M. Yang, *Science* **2019**, *364*, 1068–1075.
[30] A. Sadaf, J. S. Mortensen, S. Capaldi, E. Tikhonova, P. Hariharan, O. Ribeiro, C. J. Loland, L. Guan, B. Byrne, P. S. Chae, *Chem. Sci.* **2016**, *7*, 1933–1939.
[31] J. L. Rubinstein, *Methods (San Diego, Calif.)* **2007**, *41*, 409–416.
[32] M. Liao, E. Cao, D. Julius, Y. Cheng, *Nature* **2013**, *504*, 107–112.
[33] N. Nelson, A. Ben-Shem, *BioEssays* **2005**, *27*, 914–922.
[34] P. Jordan, P. Fromme, H. T. Witt, O. Klukas, W. Saenger, N. Krauss, *Nature* **2001**, *411*, 909–917.
[35] J. Li, N. Hamaoka, F. Makino, A. Kawamoto, Y. Lin, M. Rögner, M. M. Nowaczyk, Y. H. Lee, K. Namba, C. Gerle, G. Kurisu, *Commun. Biol.* **2022**, *5*, 1–13.
[36] A. Iudin, P. K. Korir, S. Somasundharam, S. Weyand, C. Cattavitello, N. Fonseca, O. Salih, G. J. Kleywegt, A. Patwardhan, *Nucleic Acids Res.* **2023**, *51*, D1503–D1511.
[37] O. Çoruh, A. Frank, H. Tanaka, A. Kawamoto, E. El-Mohsnawy, T. Kato, K. Namba, C. Gerle, M. M. Nowaczyk, G. Kurisu, *Commun. Biol.* **2021**, *4*, 1–16.
[38] C. Gerle, Y. Misumi, A. Kawamoto, H. Tanaka, H. Kubota-Kawai, R. Tokutsu, E. Kim, D. Chorev, K. Abe, C. V. Robinson, K. Mitsuoka, J. Minagawa, G. Kurisu, *Biochim. Biophys. Acta Bioenerg.* **2023**, *1864*, 148986.
[39] G. Young, N. Hundt, D. Cole, A. Fineberg, J. Andrecka, A. Tyler, A. Olerinyova, A. Ansari, E. G. Marklund, M. P. Collier, S. A. Chandler, O. Tkachenko, J. Allen, M. Crispin, N. Billington, Y. Takagi, J. R. Sellers, C. Eichmann, P. Selenko, L. Frey, R. Riek, M. R. Galpin, W. B. Struwe, J. L. P. Benesch, P. Kukura, *Science* **2018**, *360*, 423–427.
[40] A. Olerinyova, A. Sonn-Segev, J. Gault, C. Eichmann, J. Schimpf, A. H. Kopf, L. S. P. Rudden, D. Ashkinadze, R. Bomba, L. Frey, J. Greenwald, M. T. Degiacomi, R. Steinhilper, J. A. Killian, T. Friedrich, R. Riek, W. B. Struwe, P. Kukura, *Chem* **2021**, *7*, 224–236.
[41] W. Kühlbrandt, *Annu. Rev. Biochem.* **2019**, *88*, 515–549, DOI 10.1146/annurev-biochem-013118-110903.
[42] W. Junge, N. Nelson, *Annu. Rev. Biochem.* **2015**, *84*, 631–657, DOI 10.1146/annurev-biochem-060614-034124.
[43] J. E. Walker, *Biochem. Soc. Trans.* **2013**, *41*, 1–16.
[44] G. Pinke, L. Zhou, L. A. Sazanov, *Nat. Struct. Mol. Biol.* **2020**, *27*, 1077–1085, DOI 10.1038/s41594-020-0503-8.
[45] T. E. Spikes, M. G. Montgomery, J. E. Walker, *Proc. Natl. Acad. Sci. USA* **2020**, *117*, 23519–23526, DOI 10.1073/pnas.2013998117.
[46] Y. Lai, Y. Zhang, S. Zhou, J. Xu, Z. Du, Z. Feng, L. Yu, Z. Zhao, W. Wang, Y. Tang, X. Yang, L. W. Guddat, F. Liu, Y. Gao, Z. Rao, H. Gong, *Mol. Cell* **2023**, *83*, 2137–2147, DOI 10.1016/J.MOLCEL.2023.04.029.
[47] K. M. Davies, B. Daum, *Biochem. Soc. Trans.* **2013**, *41*, 1227–1234.
[48] N. R. Ader, P. C. Hoffmann, I. Ganeva, A. C. Borgeaud, C. Wang, R. J. Youle, W. Kukulski, *eLife* **2019**, *8*, 1–27, DOI 10.7554/ELIFE.40712.
[49] A. Urbani, V. Giorgio, A. Carrer, C. Franchin, G. Arrigoni, C. Jiko, K. Abe, S. Maeda, K. Shinzawa-Itoh, J. F. M. Bogers, D. G. G. McMillan, C. Gerle, I. Szabò, P. Bernardi, *Nat. Commun.* **2019**, *10*, 4341–4352, DOI 10.1038/s41467-019-12331-1.
[50] W. Kühlbrandt, *Microscopy* **2022**, *71*, I30–I50.
[51] S. J. Piper, R. M. Johnson, D. Wootten, P. M. Sexton, *Chem. Rev.* **2022**, *122*, 13989–14017.
[52] A. Godoy-Hernandez, A. H. Asseri, A. J. Purugganan, C. Jiko, C. de Ram, H. Lill, M. Pabst, K. Mitsuoka, C. Gerle, D. Bald, D. G. G. McMillan, *ACS Cent. Sci.* **2022**, *9*, 494–507, DOI 10.1021/acscentsci.2c01170.
[53] L. Ghani, S. Kim, M. Ehsan, B. Lan, I. H. Poulsen, C. Dev, S. Katsube, B. Byrne, L. Guan, C. J. Loland, X. Liu, W. Im, P. S. Chae, *Chem. Sci.* **2023**, *14*, 13014–13024.
[54] X. You, X. Zhang, J. Cheng, Y. Xiao, J. Ma, S. Sun, X. Zhang, H. W. Wang, S. F. Sui, *Nature* **2023**, *616*, 199–206.
[55] L. Dietrich, A.-N. A. Agip, A. Schwarz, C. Kunz, W. Kühlbrandt, **2024**, *bioRxiv* preprint DOI: 10.1101/2024.03.27.586927.
[56] X. Tao, C. Zhao, R. & MacKinnon, *Proc. Natl. Acad. Sci. USA* **2023**, *120* (18), e2302325120.
[57] C. E. Coupland, R. Karimi, S. A. Bueler, Y. Liang, G. M. Courbon, J. M. Di Trani, C. J. Wong, R. Saghian, J.-Y. Youn, L.-Y. Wang, J. L. Rubinstein, *Science* **2024**, *385*, 168–174, 10.1126/science.adp5577.
[58] J. Abramson, J. Adler, J. Dunger, et al., *Nature* **2024**, *630*, 493–500, https://doi.org/10.1038/s41586-024-07487-w.
[59] K. Abe, M. Ozako, M. Inukai, Y. Matsuyuki, S. Kitayama, C. Kanai, C. Nagai, C. C. Gopalasingam, C. Gerle, H. Shigematsu, N. Umekubo, S. Yokoshima, A. Yoshimori, *Commun. Biol.* **2023**, *6*, 3–5.
[60] D. N. Mastronarde, *Microsc. Microanal.* **2018**, *24*, 864–865, DOI 10.1017/s1431927618004816.
[61] K. Yonekura, S. Maki-Yonekura, H. Naitow, T. Hamaguchi, K. Takaba, *Commun. Biol.* **2021**, *4*, 1–8.
[62] D. Kimanius, L. Dong, G. Sharov, T. Nakane, S. H. W. Scheres, *Biochem. J.* **2021**, *478*, 4169–4185.

Manuscript received: April 1, 2024
Revised manuscript received: May 31, 2024
Accepted manuscript online: June 17, 2024
Version of record online: August 6, 2024

Correction added on 21.08.2024, after first online publication: Information for references 27 and 55 has been updated